energy&fuels

pubs.acs.org/EF

Article

Gasoline Synthesis from Biomass-Derived Syngas Comparing Different Methanol and Dimethyl Ether Pathways by Process Simulation, Based on the Bioliq Process

Mahsa E-Moghaddam,* Nicolaus Dahmen,* Ulrike Santo, and Jörg Sauer

Cite This: https://doi.org/10.1021/acs.energyfuels.3c04524

Read Online

ABSTRACT: In the bioliq process, biomass is converted to gasoline over four steps including pyrolysis, synthesis gas (syngas) generation via gasification, gas cleaning, and gasoline synthesis via dimethyl ether (DME). This work aims to investigate the gasoline synthesis plant of the bioliq process and also alternative process routes for the conversion of biomass-derived syngas to gasoline via methanol (MeOH) and DME pathways by process simulation in Aspen Plus, using a syngas composition adapted from the bioliq plant and enhanced with makeup H_2. The simulations were established using kinetic models for MeOH, DME, and water−gas shift (WGS) synthesis based on selected models from the literature and component yield models for MeOH/DME to gasoline (MTG/DTG) reactions based on product characteristics from known gasoline synthesis plants. The selected process routes were compared regarding product mass and energetic efficiencies and H_2 and CO_2 balances. The results showed that an optimized bioliq process, i.e., biofuel synthesis via direct DME synthesis with a WGS unit for makeup H_2 supply, is efficient in terms of syngas conversion and gasoline productivity, although it has a drawback concerning CO_2 generation. For this process, the mass and chemical energy efficiencies of gasoline based on syngas were calculated to be approximately 15 and 65%, respectively. Comparatively, for the similar process via the MeOH pathway, these efficiencies were found to be 11 and 50%, respectively. The CO and H_2 conversion rates for gasoline synthesis via DME were found to be about 77 and 64%, respectively, whereas via MeOH, they were obtained as ca. 48 and 28%, respectively. Additionally, the optimized process was scaled up for production of 100,000 tons/year gasoline and evaluated based on mass and chemical energy and CO_2 and element (hydrogen, carbon, and oxygen) balances. Here, the mass and chemical energy efficiencies of gasoline based on biomass feed were calculated to be 13 and 35%, respectively.

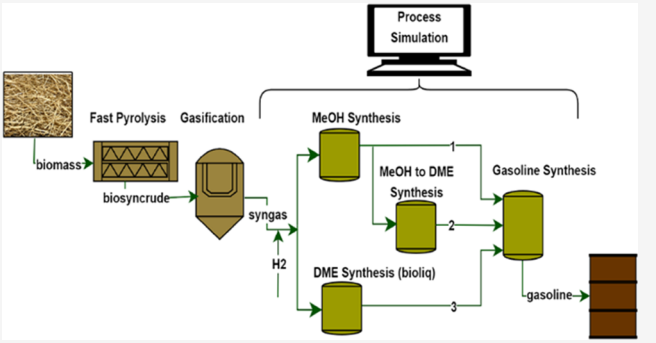

1. INTRODUCTION

The substitution of fossil feedstock is mandatory to reduce greenhouse gas emissions. Also, the worldwide increasing demand for transportation fuels calls for more oil and gas extraction, and as is well known, these resources are limited. Developing new fuel synthesis technologies using renewable carbonaceous materials such as biomass can help overcome the energy shortage especially in the countries with no fossil fuel reserves. Beyond the established first-generation biofuels produced from sugar, starch, and vegetable oil, lignocellulosic biomass as the most abundant biomass resource can be converted into energy carrier chemicals and sustainable biofuels. Second-generation biofuels, also known as advanced biofuels, as promising alternatives to fossil fuels, have gained momentum in the renewable energy sector in recent decades. These kinds of fuels are produced from agricultural, forest, or biomass processing residues, which do not compete with food and feed production.[1] The conversion of biomass-to-liquid (BTL) fuels is typically proceeded using three main processes of pyrolysis, gasification, and liquefaction, each with advantages and disadvantages.[2]

The bioliq process[3−5] developed at the Karlsruhe Institute of Technology (KIT) aims to convert biomass residues into synthetic fuels. The pilot plant with a thermal fuel conversion capacity of 2−5 MW consists of four main stages: fast pyrolysis, a high-pressure entrained flow gasifier, intensive hot gas cleaning to remove undesired sour gases (HCl, H_2S, and partly CO_2) and trace compounds (e.g., HCN, NH_3), and a synthesis plant for gasoline production via DME. In general, depending on the type of feedstock and desired conversion capacity, dry lignocellulosic biomass can be converted into

Received: November 16, 2023
Revised: January 29, 2024
Accepted: February 1, 2024

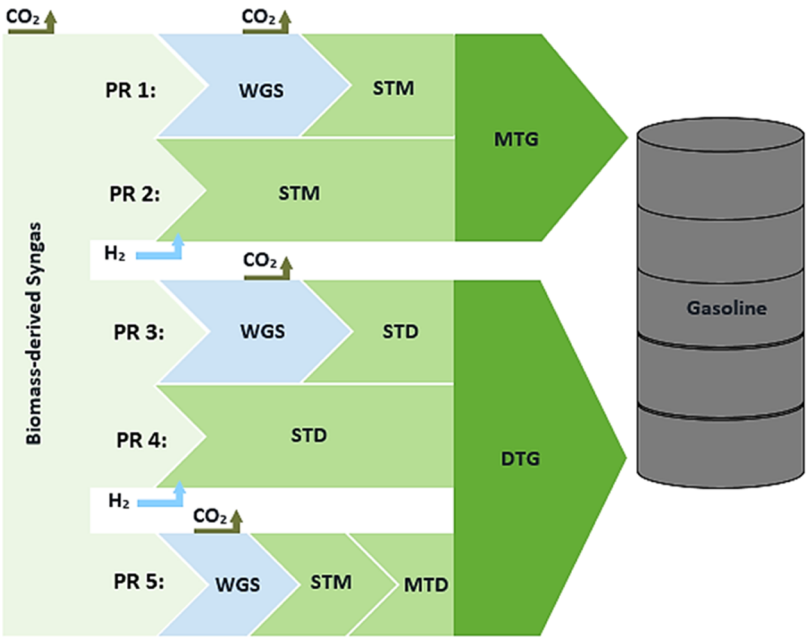

Figure 1. Selected process routes (PRs) for gasoline synthesis from biomass-derived syngas in this work. PR 1: MeOH synthesis with H_2 from the internal WGS unit, PR 2: MeOH synthesis with H_2 from the external source, PR 3: direct DME synthesis with H_2 from the internal WGS unit, PR 4: direct DME synthesis with H_2 from the external source, and PR 5: indirect DME synthesis with H_2 from the internal WGS unit.

synthesis gas (a mixture of mainly CO, H_2, some CO_2, and H_2O) by a number of gasification technologies.[6] The elemental analysis of lignocellulosic biomass varies, depending on the type, age, and origin of the material. In the case of wheat straw (dry), the carbon, hydrogen, and nitrogen content is approximately 43−44, 6−6.2, and 0.6 wt %, respectively.[7] Widely distributed biomass residues of low volumetric energy density like cereal straw are first converted into an energy-dense energy carrier by fast pyrolysis, as described elsewhere.[8,9] Next, the combined solid and liquid pyrolysis products, termed biosyncrude, are transported to a large industrial site for gasification and synthetic fuel production.

The conversion of biomass-derived syngas to fuels can be accomplished using different methods. These include Fischer−Tropsch (FT) synthesis,[10,11] MeOH synthesis[12,13] followed by a MeOH to gasoline (MTG) process like ExxonMobil,[14] or DME synthesis[15,16] followed by a DME to gasoline (DTG) process such as Topsoe integrated gasoline synthesis (TIGAS).[17] Various studies exist in the literature that examine the BTL process through different pathways using experimental data or modeling and simulation tools. For instance, Kim et al.[18] investigated a pilot-scale BTL process for producing diesel through FT synthesis, comparing it to standard automotive diesel. Their report also provides information about the worldwide research status of biofuel production through FT synthesis. Baliban et al.[19] used mathematical optimization modeling to economically investigate different BTL processes through multiple technologies including FT, MTG, and MeOH to olefin (MTO). They considered different biomass feedstocks and achieved nearly identical overall energy efficiencies (including electricity) in their work. Trippe et al.[20] conducted a techno-economic assessment of the BTL process, evaluating both the DTG and FT routes using simulation. According to their study, the energy efficiencies (including electricity) from biomass and also syngas to final products (gasoline and diesel) are slightly higher for the FT compared to the DTG route. Gonzalez et al.[21] have compared the BTL process for FT and MTG pathways and found that the biofuel energy efficiency via FT synthesis is higher than that via MTG synthesis. Also, the carbon efficiency in the FT route is slightly higher because of the formation of lighter hydrocarbons (C_1−C_4) in FT synthesis. Similarly, Dimitriou et al.[22] have investigated the three mentioned configurations for the BTL process via woody biomass gasification. According to their techno-economic analysis, the FT synthesis technology is more efficient than the MTG and DTG (TIGAS) pathways for commercial production. The calculated biofuel energy efficiency and mass yield (with respect to biomass) in their work are as per the following order: FT > DTG > MTG.

However, it should be noted that the product from the MTG/DTG pathways compared to that from the FT pathway has a higher selectivity of gasoline-range hydrocarbons and accordingly does not necessarily need upgrading to be usable as transportation biofuel.[23] Therefore, this remark should be taken into account when comparing the FT to MTG/DTG process routes. Moreover, the FT route in commercial application is economically unfeasible due to the related high investment cost.[24]

In comparison with the aforementioned studies and in the context of the bioliq process development, we examine the production of the gasoline product from biomass-derived syngas via the MTG (ExxonMobil) and DTG (TIGAS) pathways. The objective of this study is to simulate the bioliq process by applying optimized conditions to the initial base case process. Using this optimized model, we assess the potentials of the process also through the MeOH pathway, considering the integration of makeup H_2 into biomass-derived syngas. The scientific contribution of this work lies in conducting a comparative simulation analysis of different process routes for gasoline production from biomass-derived syngas, in terms of mass and energetic efficiencies as well as hydrogen and carbon dioxide balance, an area that, to the best of the authors' knowledge, is limited in the available literature.

https://doi.org/10.1021/acs.energyfuels.3c04524
Energy Fuels XXXX, XXX, XXX−XXX

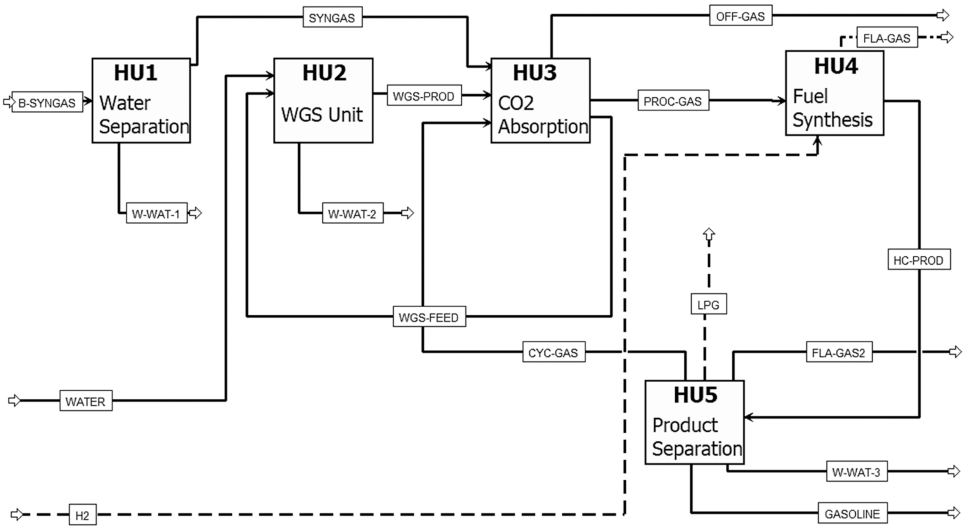

Figure 2. Simulation flowsheet. Hierarchy units (HUs): HU1: water separation; HU2: water−gas shift reaction, HU3: CO_2 absorption and desorption, HU4: MeOH/DME and gasoline synthesis; and HU5: product separation. Stream labels: B-SYNGAS: biomass-derived syngas; CYC-GAS: cycle gas in the STD pathway process; LPG: liquefied petroleum gas in the STM pathway process; FLA-GAS: flare gas; HC-PROD: hydrocarbon product mixture; GASOLINE: gasoline product; OFF-GAS: CO_2-rich gas; PROC-GAS: treated feed to the reaction unit; WGS-FEED: syngas split to the WGS unit; WGS-PROD: H_2-rich syngas; and W-WAT: wastewater.

The findings will facilitate the identification of the most promising process constellations concerning different optimization targets. Furthermore, this work contributes to kinetic-based simulations for the production of intermediate products, followed by predicting the quantity of synthesized gasoline in the simulated process routes.

2. METHODS

2.1. Selected Process Routes. The investigated process routes (PRs) are depicted in Figure 1. The process routes 1 and 2 illustrate the conversion of syngas to gasoline (STG) via the MeOH synthesis pathway; a well-known industrial example for this case is the MTG process run by ExxonMobil. The process routes 3−5 indicate the conversion of syngas to gasoline via direct and indirect DME synthesis. Direct DME synthesis from the syngas (STD) process involves the syngas to MeOH (STM) and MeOH to DME (MTD) conversions occurring within a single reactor. This process represents an optimized bioliq-type plant that has not been yet developed to an industrial scale. In the indirect synthesis process, MeOH is produced as an intermediate product that can be directly transferred to the MTD reactor or stored for later conversion to DME. Since biomass-derived syngas from the bioliq plant, similar to other typical biomass gasification processes, most often has H_2/CO ratios below 1, makeup H_2 can be added to the feed to maximize carbon conversion and enhance productivity in STM and STD reactors. The required makeup H_2 could be provided from processes such as steam methane reforming, water electrolysis, or the WGS reaction. In this work, two cases for the H_2 supply source have been considered: an internal WGS unit in the plant, used in the process routes 1, 3, and 5 and an external source that supplies the plant directly with H_2, in process routes 2 and 4.

In addition, by employing the simulation model of PR 3, which essentially represents an optimized bioliq process, the scaling up of the process was conducted to facilitate a future techno-economic analysis.

2.2. Process Configuration and Simulation. The steady-state simulation of the selected process routes was established in Aspen Plus V10 software in hierarchical models using the plant design information on the current bioliq process as a basis. Figure 2 illustrates the overall simulation flowsheet. Subprocess units from biomass-derived syngas to gasoline are simulated individually in five hierarchy units (HUs), as can be observed in the figure. The hierarchy units are assembled into each process route simulation based on the objective of each process. Following the bioliq plant concept, syngas leaving the gasifier, having completed some cleaning steps, proceeds to the first step of the synthesis site (HU1). Here, syngas undergoes cooling and then dehydration through a two-phase separator at ambient temperature. The syngas feed composition, namely, the H_2/CO ratio and CO_2 fraction, is adjusted by means of makeup H_2, either from the external H_2 source or the internal WGS unit (HU2) and the CO_2 absorption unit (HU3). The CO_2 content of water-free fresh syngas (ca. 15−18 vol % in the bioliq plant) should be reduced for MeOH/DME synthesis. In HU3, two packed bed absorbers are situated to absorb CO_2 from fresh syngas and also cycle gas (unconverted gases leaving the reaction unit (HU4)) by employing poly(ethylene glycol) dimethyl ether (PEG) as the solvent. Syngas and the solvent flow counter-currently through the column and the loaded solvent is directed to a regeneration column or desorber. CO_2-reduced syngas (6−7 vol %) is transferred to the reaction unit and CO_2-rich off-gas is exhaled from the desorber effluent. The reactors for MeOH/DME and gasoline synthesis are situated in HU4. The product mixture out of this unit is transferred to HU5 to be separated to gasoline, water, and gases through a three-phase separator. In the bioliq plant, after the separation unit, a gasoline stabilization unit is located to separate light and heavy fractions via a packed bed distillation column. However, in this work, as the bioliq process was optimized, the composition of the gasoline product was adapted from the ExxonMobil MTG process, closely resembling that of standard gasoline. Therefore, the stabilization unit is omitted here, and the process is only until raw gasoline investigated.

Each simulation consists of four or five hierarchy units depending on the makeup H_2 source. If H_2 is supplied from an external source, HU2 is eliminated and H_2 is directly added to the feed line to the reaction unit (HU4). In the case of STD synthesis (PRs 3 and 4), unconverted syngas from DME synthesis, which is rich in CO_2, should be again treated in the CO_2 absorption unit for further conversion in the STD reactor and hence is returned to HU3 through the CYC-GAS line. For the STM process, this line is removed and since unconverted gas from MeOH synthesis does not need more treatment, the gas is directly recycled to the STM reactor. Also, here, the product of the gasoline synthesis reactor contains only a small gas flow rate of liquefied petroleum gas (LPG) as the byproduct of the MTG process that is separated through the product separation unit (HU5). For this work, the concept of the MeOH synthesis segment has been adapted from the low-pressure MeOH synthesis process of

https://doi.org/10.1021/acs.energyfuels.3c04524
Energy Fuels XXXX, XXX, XXX−XXX

Lurgi.[14] Individual overall flowsheets for the selected process routes and the flowsheets of HU1−HU5 for PR 3 can be found in the Supporting Information.

The property method of each hierarchy unit is selected based on the component type, process condition, and objective. For HU1 and HU5, the PENG-ROB method and for HU2 and HU4, the SRK method were used. These two equation of state methods are extensively used for hydrocarbon mixture systems in oil, gas, and petrochemical processes, as also suggested by the Property Method Selection Assistant in Aspen Plus. For HU3, the well-proven equation of state model of PC-SAFT has been employed. This model can predict the properties of systems that include syngas and physical solvents like PEG. The binary interaction parameter sets for PEG were modified in Aspen Plus according to the reported data by the MIT Energy Initiative.[25]

Besides the uniform simulation models, using identical assumptions and considerations is significant to ensure a reliable comparison between the selected process routes. The syngas feed composition as well as process conditions such as pressure, temperature, vapor fractions, material stream properties, and purities have been collected from a bioliq test campaign. If optimization was required for a unit, the data were modified based on existing industrial cases found in the literature. In the following, the methods and considerations taken for the feed and simulation of the reaction subunits are discussed.

2.3. Theoretical Background and Considerations. The process routes represented in Figure 1 have been simulated by using kinetic models for MeOH, DME, and WGS syntheses and component yield-based models for MTG and DTG syntheses. The relevant reactions are given below in eqs 1−5.

$$CO_2 + 3H_2 \rightleftharpoons CH_3OH + H_2O \quad (1)$$

$$CO + 2H_2 \rightleftharpoons CH_3OH \quad (2)$$

$$CO + H_2O \rightleftharpoons CO_2 + H_2 \quad (3)$$

$$2CH_3OH \rightleftharpoons CH_3OCH_3 + H_2O \quad (4)$$

$$CH_3OCH_3/CH_3OH + H_2O \rightarrow C_{1-2} + C_{3-4}(\text{LPG}) + C_{5^+}(\text{gasoline}) + H_2O \quad (5)$$

In the comparative simulations for the process routes 1 to 5, the same syngas feed flow rate (551 kg/h) and also the identical feed composition, given in Table 1 (first row), were used. The syngas composition was adapted from a selected bioliq plant operation campaign. The N_2 content was reduced because the presence of N_2 generally decreases feed conversion, potentially leading to non-representative results. In the current bioliq plant, the N_2 content of syngas is higher than that expected for a commercially operated plant due to practical requirements of gasifier operation in upstream.

Table 1. Feed Composition Used in the Simulations in This Work

component	H_2	CO	CO_2	N_2	H_2O	CH_4
composition (mol %) in the selected process routes 1−5	35.0	36.0	18.0	3.0	6.0	2.0
composition (mol %) in the scaled-up bioliq process	22.2	24.7	10.6	0.4	42.0	0.0

In the process simulation for scaling up the optimized bioliq process, an optimized syngas feed composition, also given in Table 1 (second row), was employed. In this case, the feed composition was estimated via process simulations of the pyrolysis and gasification units of the bioliq process. Fast pyrolysis of wheat straw (water content: 9.5 wt %, ash content: 5.4 wt %, LHV (dry basis): 16.0 MJ/kg) was simulated to yield liquid bio-oil, aqueous condensate, and solid biocoal. All solid and liquid products were considered a feed for gasification in the form of a fuel suspension for entrained flow gasification. By-produced fuel gas from fast pyrolysis was utilized within the process. Mass and energy flows as well as syngas composition were calculated on the basis of a 500 MWth thermal fuel capacity for gasification at 40 bar, and cold gas efficiency reached 73% under these conditions. The information on feedstock, pyrolysis, and gasification products for the 500 MW case is reported in Table 2.

Table 2. Feed and Products in Pyrolysis and Gasification Simulations (on a Wet Feedstock Basis)

	straw feedstock	pyrolysis product	synthesis gas
mass flow rate (t/h)	171.1	116.8	210.5
thermal fuel capacity (MW)	675.7	500.0	365.0
LHV (MJ/kg)	14.2	15.4	6.1

At first glance, the two compositions in Table 1 appear different; however, after water removal in HU1, both compositions are quite similar in terms of the H_2/CO content and ratio.

It is generally known that for an efficient STM and STD synthesis, the composition of the feed to the reactors should fulfill the required industrial standards. Then, for the STM reaction, the proper syngas composition was assured by factors such as stoichiometric number (SN), which should be greater than 2, depicted by eq 6[33] or the H_2 fraction given by eq 7,[34] whose optimal value is 1.05.[35] For the STD reactor, the H_2/CO ratio in the feed was adjusted to 1.3.[17]

$$SN = \frac{\dot{n}_{H_2,in} - \dot{n}_{CO_2,in}}{\dot{n}_{CO,in} + \dot{n}_{CO_2,in}} \quad (6)$$

$$H_2 \text{ fraction} = \frac{\dot{n}_{H_2,in}}{2\dot{n}_{CO,in} + 3\dot{n}_{CO_2,in}} \quad (7)$$

It should be noted that in the simulations, the minimum possible amount of required H_2 for efficient STM/STD synthesis has been used. When eq 2 (two times) and eqs 3 and 4 are considered for DME synthesis, the net reaction is as in eq 8, and accordingly the stoichiometric H_2/CO ratio is 1. Knowing that eq 2 is actually the sum of eqs 1 and 3, the DME synthesis process can be defined as two times eq 1 and three times eq 3 plus eq 4. However, if the WGS reaction (eq 3) is accomplished two times, the net reaction will be as in eq 9, with a H_2/CO ratio of 2. Then, it can be inferred that the actual net reaction likely lies between these two equations. This inference depends on factors such as the available syngas composition, operating conditions, progression of the WGS reaction, and the composition of employed catalysts in the catalyst mixture system.

$$3CO + 3H_2 \leftrightarrow CH_3OCH_3 + CO_2 \quad (8)$$

$$2CO + 4H_2 \leftrightarrow CH_3OCH_3 + H_2O \quad (9)$$

Therefore, in STD synthesis, consideration of H_2/CO ratios above 1 can ensure improved syngas conversion rates. As also evident in the work of Song et al.,[36] increasing the ratio to 1.3 leads to an increase in the CO conversion and DME yield. Also, other authors[15,37−40] have experimentally found that the H_2/CO ratios up to 2 enhance the conversion rate when the feed contains CO_2 in addition to H_2 and CO. In addition, when the catalyst system comprises a larger fraction of MeOH and the WGS synthesis catalyst compared to the MeOH dehydration catalyst, CO conversion increases. For instance, a catalyst ratio of 75:25 wt % compared to 50:50 wt % was found to be more efficient.[15,41]

According to the the NREL report, in STM synthesis, the allowed mole fraction of CO_2 in the feed ranges from 3 to 8 mol % and values up to 7% increase MeOH productivity.[42] In STD synthesis, keeping low concentrations of CO_2 in the feed at 4−6 mol % has a positive impact on DME productivity; however, higher amounts reduce CO conversion due to the influence on the WGS reaction.[41] Besides, it has been reported that the presence of CO_2 in the feed reduces the maximum temperature in the reactor bed, thereby ensuring a safer

https://doi.org/10.1021/acs.energyfuels.3c04524
Energy Fuels XXXX, XXX, XXX−XXX

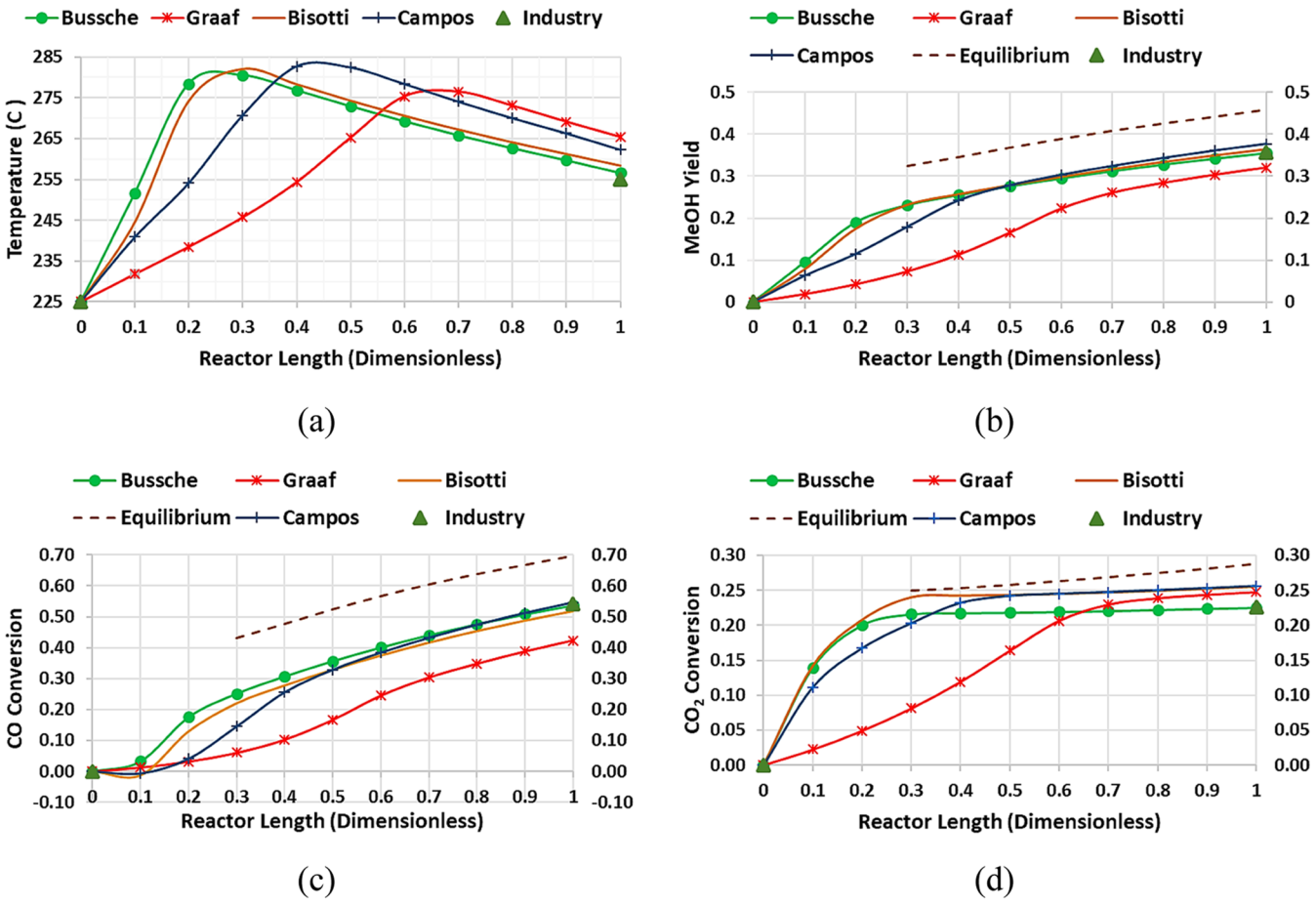

Figure 3. STM reactor simulation: comparison of (a) temperature profile, (b) Y_{MeOH}, (c) X_{CO}, and (d) X_{CO2} in selected kinetic models, with industrial data. Reaction conditions: P = 67 bar, SN = 2.1, and CO_2 mol % = 7.5.

operation.[36] Here, the CO_2 mole fraction was adjusted within a range of 7.0−7.5 and 6.0−6.5% in the STM and STD reactors, respectively.

The type of kinetic reactors was considered a fixed bed tubular reactor, in which the feed flows axially through the catalyst-filled tubes and the reaction heat is removed by boiling feedwater, which flows on the shell side and leaves the reactor as a medium pressure steam.[43] In the simulation, the *RPlug* model for reactors and the *Flash2* model for the cooling medium (steam drum) are typically employed. For simulating the behavior of catalysts in reactors, the Langmuir−Hinshelwood−Hougen−Watson (LHHW) mechanism has been applied. Then, the reaction rates were calculated based on the LHHW kinetic expression in Aspen Plus, as defined by eqs 10−13. Besides, the simulated kinetic reactor models were validated against available industrial data to ensure the accuracy of the developed models in simulation.

$$r = \frac{[\text{kinetic factor}][\text{driving force expression}]}{[\text{adsorption expression}]} \tag{10}$$

$$\text{kinetic factor} = k\left(\frac{T}{T_0}\right)^n \exp\left(-\left(\frac{E}{R}\right)\left(\frac{1}{T}-\frac{1}{T_0}\right)\right) \tag{11}$$

$$\text{driving force} = k_1 \prod_{i=1}^{N} C_i^{ai} - k_2 \prod_{i=1}^{N} C_j^{bj} \tag{12}$$

$$\text{adsorption term} = \sum_{i=1}^{M} K_i \left(\prod_{j=1}^{N} C_j^{mij}\right) \tag{13}$$

For simulating MTG/DTG reactors, the *RYield* model was employed using available product distribution and composition in literature.[14,17,42] The validity of the assumed data was evaluated by performing atom balance (for elements of hydrogen, carbon, and oxygen) over the reactors and also over the overall synthesis plant boundary, using the indicated inlet and outlet streams, as shown in Figure 2. For this work, the raw gasoline composition data of the bioliq plant were not used in the simulation of the DTG reactor due to its high aromatic content. The operational limitations of the current plant influences the gasoline quality. For instance, the pressure in the DTG reactor is about 30−35 bar and it is stated that pressure plays an important role in aromatic formation.[44−46] Golubev et al.[46] examined the pressure effect on DME conversion over a commercial zeolite-containing catalyst and found that raising the pressure from 1 to 30 bar sharply increases the yield of aromatic components.

2.4. Process Evaluation and Efficiencies. For the sake of fair comparison between the process routes, the amount of gas hourly space velocity (GHSV), as represented in eq 14, in the STM and STD reactors was considered analogous in the range of 12,300−12,400 (1/h). Also, the reaction residence time and the feed conversion rate were kept equivalent between the identical process routes with different makeup H_2 sources, i.e., between PRs 1 (or 5) and 2 in the STM reactor and between PRs 3 and 4 in the STD reactor. The reactant conversion and product yield were assessed according to eqs 15 and 16.

$$\text{GHSV} = \dot{V}_{\text{feed,st}}/V_{\text{cat}} \tag{14}$$

$$X_{\text{Rea}} = \left(1-\frac{\dot{n}_{\text{Rea,out}}}{\dot{n}_{\text{Rea,in}}}\right)\cdot 100;\ \text{Rea: CO, CO}_2\text{, H}_2 \tag{15}$$

https://doi.org/10.1021/acs.energyfuels.3c04524
Energy Fuels XXXX, XXX, XXX−XXX

$$Y_{Pro} = \left(\frac{a\dot{n}_{Pro,out}}{\dot{n}_{CO,in} + \dot{n}_{CO_2,in}}\right)\cdot 100;\ \text{Pro: MeOH, DME}$$

a: 1 for MeOH and 2 for DME (16)

The process routes were evaluated in terms of the product mass yield and chemically bound energy flows. The mass efficiency (η_{mass}), given by eq 17, was calculated for the intermediate products of MeOH and DME, and the finished product of gasoline with respect to syngas feed to the plant. The chemical energy conversion efficiency (η_{LHV}) was calculated for gasoline with respect to syngas and also carbon, based on the lower heating value (LHV) of components, as defined by eq 18.[47] Syngas in the equations accounts for the added hydrogen in PRs 2 and 4.

$$\eta_{mass} = \frac{\dot{m}_{Pro}}{\dot{m}_{Ref}};\ \text{Pro: MeOH, DME, gasoline}$$

Ref: syngas (17)

$$\eta_{LHV} = \frac{\dot{m}_{Pro} \times LHV_{Pro}}{\dot{m}_{Ref} \times LHV_{Ref}};\ \text{Pro: gasoline}$$

Ref: syngas, carbon (18)

3. SIMULATION OF REACTION SUBUNITS

3.1. Methanol Synthesis from Syngas (STM). The reaction mechanism and the kinetics of the syngas to MeOH conversion process over the $CuO/ZnO/Al_2O_3$ catalyst has been investigated by several authors with different viewpoints regarding the source of carbon for MeOH synthesis, whether this is CO, CO_2, or both components.[13,48,49] Among the studies which consider MeOH synthesis from both CO_2 and CO (eq 1, eq 2, and reverse of eq 3), the work of Graaf et al.[26−28] and among the works assuming MeOH synthesis only from CO_2 (eq 1 and reverse of eq 3), the work of Bussche et al.[29] were selected. Bussche et al. integrated the equilibrium data of Graaf et al. in their original kinetic model, and as later in 2016, Graaf and his colleague proposed optimized equilibrium constant relationships for MeOH synthesis;[50] the new equations can replace the old ones. However, using the optimized equilibrium equations in Aspen Plus holds some uncertainties because all terms of the equation cannot be inserted in the simulation and only a truncated equation in the form of $A + B/T + C \ln T + DT$ can be executed. Therefore, to have a precise simulation result, the old equilibrium data were used in both models.

Beside these two kinetic models, which are extensively used in STM reactor modeling, two other models have also been investigated: a model proposed by Bisotti et al.,[51,52] which essentially is a refitted Graaf model, and a model by Campos et al.,[53] developed based on density functional theory (DFT) calculations. The Campos model, similar to the Bussche model, also considers the source of carbon from CO_2. The four kinetic models were simulated and the validity of the simulations was tested on an industrial Lurgi-type reactor, located at the Tuha Oilfield Company.[54,55] The results of simulations along with the industrial data are demonstrated in Figure 3, and for the sake of clarity, the percentage errors are provided in Table 3. It can be seen that the Bussche model compared to the Graaf model is in a better agreement with the industrial plant data. The Graaf model underestimates methanol production, as also reported by other authors.[48,56] Bisotti et al. have refitted the Graaf model and proposed new data, and according to their report, the new model for the simulation of industrial reactors is more reliable than the Bussche model. However, the result of this work has indicated that although the refitted model compared to the original Graaf model can better predict the process, the Bussche model still shows more accuracy. The Campos model also produces good results, particularly in terms of CO conversion.

Table 3. STM Reactor Simulation and Percentage Error between the Industrial Data and Simulated Models in This Work

parameters	Bussche (%)	Graaf (%)	Bisotti (%)	Campos (%)
T_{out}	0.6	4.1	1.3	2.8
X_{CO}	0.8	21.8	4.5	0.9
X_{CO2}	0.3	9.5	13.0	13.3
Y_{MeOH}	0.5	10.1	2.1	5.6

3.2. DME Synthesis from MeOH (MTD). Methanol is dehydrated to DME over the acidic alumina catalysts, $\gamma-Al_2O_3$, modified alumina, or zeolite-type catalysts such as H-ZSM-5 and H−Y-zeolite.[57] Here, for the simulation of the MTD reactor, the kinetics of the $\gamma-Al_2O_3$ catalyst was investigated due to its usage in the bioliq plant. Also, this catalyst is employed in the Lurgi MegaDME process, according to which a methanol conversion of 70−85% is typically achieved at temperatures of 250−360 °C.[58] The kinetic data from Bercic et al.[30] and equilibrium constants from Diep et al.[31] were selected, and the validation of the kinetic simulation was verified by simulating an industrial MTD adiabatic fixed bed reactor located at the Zagros Petrochemical Company.[59,60] The simulation was performed by considering both adiabatic and isothermal scenarios. For the isothermal case, the temperature of 316 °C for the cooling medium, calculated by Farsi et al.[60] as the optimum value, was considered in the simulation. As evident from Figure 4, the simulation result of this work is in proper agreement with the industrial data and also the simulation result of Farsi et al. The percentage error data are listed in Table 4.

3.3. DME Synthesis from Syngas (STD). The direct STD conversion process in the bioliq plant is carried out using a mechanical catalyst mixture consisting of $CuO/ZnO/Al_2O_3$ and $\gamma-Al_2O_3$ catalysts. For the simulation of the STD reactor, an integrated kinetic model of STM synthesis from Bussche and MTD from Bercic was used, thanks to the precise representation of these models observed on industrial reactor verifications. Since no information on an industrial STD reactor was found, no simulation validation was possible. Then, for this simulation, syngas feed was adapted from the bioliq plant (PR 3). Also, the STD reactor in the bioliq plant, which is operated at suboptimum conditions for some reasons, was optimized in terms of pressure and temperature, and isothermal operation was considered. In addition, it is noteworthy that the temperature in the STD reaction should not go above 300 °C due to the deactivation of the $CuO/ZnO/Al_2O_3$ catalyst at higher temperatures.[61] Figure 5 shows the results of this simulation. It is evident from the figure that the outlet temperature is higher compared to that of STM synthesis (Figure 3a). Also, as expected and previously reported,[62] CO conversion via the STD reaction is higher than that via the STM reaction.

In the case of indirect DME synthesis from syngas, the produced MeOH from the first reactor might be stored for later conversion to DME, though here the simulation was established by putting both STM and MTD reactors in one

https://doi.org/10.1021/acs.energyfuels.3c04524
Energy Fuels XXXX, XXX, XXX−XXX

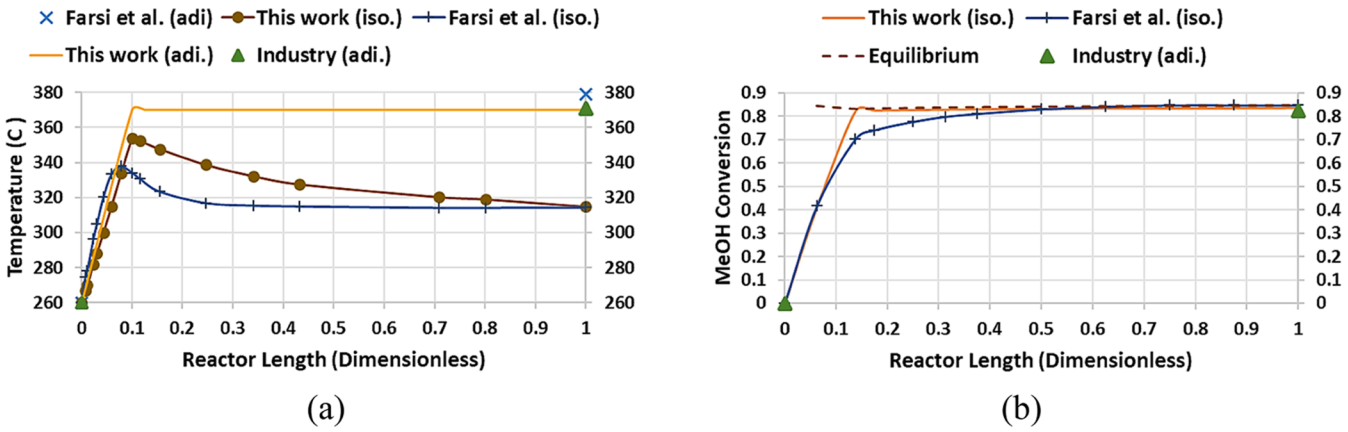

Figure 4. MTD reactor simulation: (a) temperature profile in isothermal (iso.) and adiabatic (adi.) operations and (b) X_{MeOH} in isothermal operation compared to reference data. Reaction conditions: P = 22 bar and MeOH wt % = 96. The graph of Farsi et al. was reproduced.

Table 4. MTD Reactor Simulation and the Percentage Error between the Industrial Data (Adiabatic Operation) and the Simulated Model in This Work and the Work of Farsi et al.

parameters	this work (%)	Farsi et al.[60](%)
T_{out}	0.2	2.2
X_{MeOH}	1.3	2.7

operation run for the sake of comparison with direct DME synthesis. Then, for process evaluation, one system boundary around the series STM and MTD reactors was considered. In Table 5, the direct and indirect STD conversions relevant to PRs 3 (the optimized bioliq process) and 5, respectively, are compared. It is obvious that direct DME synthesis is more productive than the indirect process, whereas CO_2 is a side product there. Consistent with this result, Mevawala et al.[63] analyzed both direct and indirect DME syntheses using simulation and found that the DME yield in the direct route (H_2/CO = 1) is higher compared to that in the indirect route. In the direct DME synthesis process, the thermodynamic limitations of MeOH synthesis in the indirect route are alleviated, leading to higher CO conversions and DME productivities.[64−66]

3.4. Water−Gas Shift (WGS) Synthesis. The well-known WGS reaction (eq 2) is thermodynamically favored at low temperatures (LTs) but kinetically favored at high temperatures (HTs). Therefore, in industry, the process is conducted in two series reactors, such that the first reactor operates at HT (280−350 °C) with the Fe_2O_3−Cr_2O_3 catalyst and the second reactor at LT (180−260 °C) with Cu-based catalysts;[67] both are operated adiabatically with an intersystem cooling between them.[68] For this work, similar to the bioliq plant concept, a one-step LT WGS process was considered and accordingly a kinetic model for the WGS reaction over the conventional $CuO/ZnO/Al_2O_3$ catalyst reported by Lu et al.[32] was selected. The simulation model was tested against an industrial LT WGS adiabatic reactor, which is situated after a HT WGS reactor in a plant layout introduced by Alhabdan.[69] The highest CO conversion occurs in the HT WGS reactor, but the HT operation also favors the RWGS reaction toward CO and water, and hence in the LT WGS reactor, the rest of the CO is converted.[69] As shown in Figure 6, the result of this simulation is compared with the industrial data and the mathematical model result of Alhabdan. The percentage error data are provided in Table 6, and as can be observed, the results are very close to the reference data. Also, from Figure 6b, it is noticeable that the conversion already reaches its maximum at the beginning of the reactor bed.

For the WGS subunit in PRs 1, 3, and 5, in order to increase CO conversion at the LT WGS kinetic model, a H_2O/CO molar ratio bigger than the stoichiometric value of 1 (ca. 1.4) was considered because it is experimentally proven that the

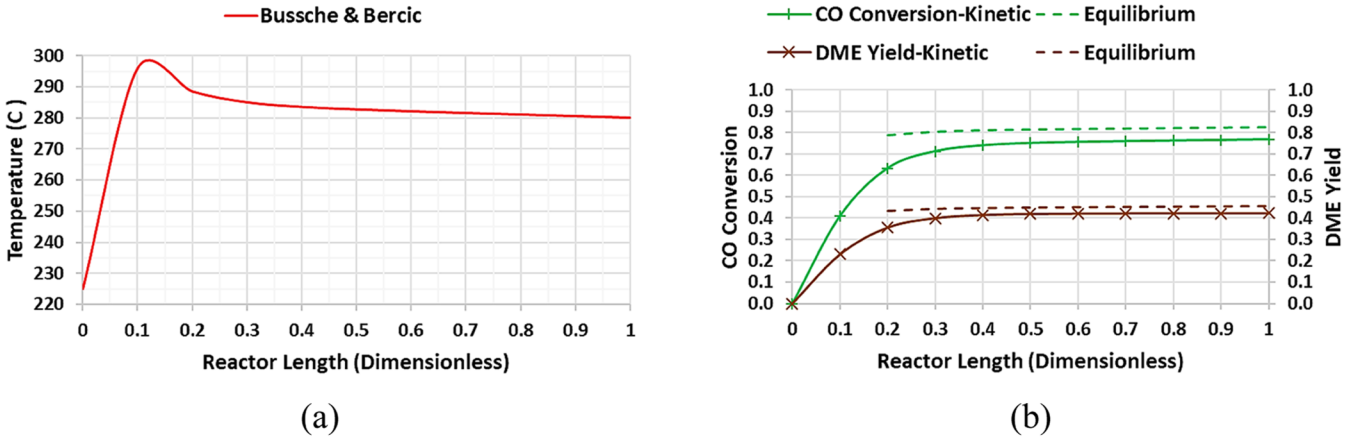

Figure 5. STD reactor simulation: (a) temperature profile and (b) X_{CO} and Y_{DME}. Reaction conditions: P = 67 bar, H_2/CO = 1.3, and CO_2 mol % = 6.1.

https://doi.org/10.1021/acs.energyfuels.3c04524
Energy Fuels XXXX, XXX, XXX−XXX

Table 5. Comparison of Direct and Indirect Syntheses of DME from Biomass-Derived Syngas

	T_{in} (°C)	P (bar)	X_{CO} (%)	X_{CO2} (%)	X_{H2} (%)	Y_{DME} (%)	T_{out} (°C)
direct (STD)	225	67	77		64	43	280
indirect (STM/MTD)	225/260	67/22	48	7	28	29	258/315

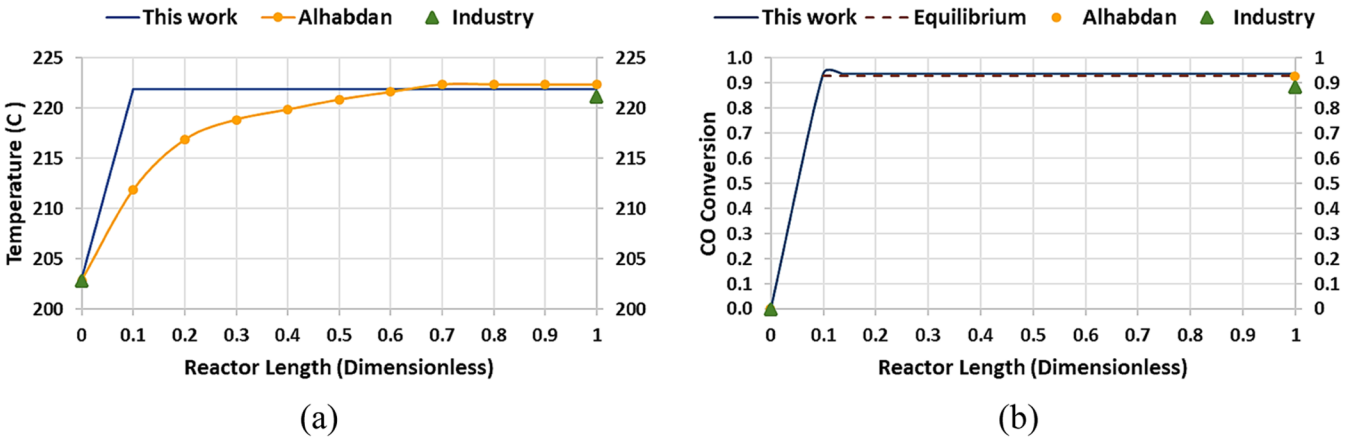

Figure 6. WGS reactor simulation: comparison of (a) temperature profile and (b) X_{CO} with reference data. Reaction conditions: P = 23 bar, H_2O/gas = 0.5, and H_2O/CO = 19.5. The graph of Alhabdan was reproduced.

Table 6. WGS Reactor Simulation and Percentage Error between the Industrial Data and the Simulated Model in This Work and the Work of Alhabdan

parameters	this work (%)	Alhabdan[69] (%)
T_{out}	0.4	0.6
X_{CO}	6.0	4.9

increase of steam to CO at constant temperature accelerates CO conversion in the process.[70,71]

3.5. Gasoline Synthesis from MeOH/DME (MTG/DTG).

The MTG reactor was simulated using the component yield model based on product distribution and composition data from the ExxonMobil MTG fixed bed pilot plant.[14] Principally, the only available complete gasoline composition was found in the DOE report, which provides a detailed mass balance with ca. 50 hydrocarbons over the MTG reactor. The feed to the plant is MeOH with a purity of 96 wt %, and the product (excluding acetone, formic acid, and coke) is a mixture of almost 58 wt % water and 42 wt % hydrocarbons consisting of approximately 80 wt % gasoline and 20 wt % light gases and LPG. For temperature control purposes in the plant, crude MeOH is first partially converted to DME in an intermediate reactor, and then an equilibrium mixture of MeOH/DME and water is introduced to the MTG reactors. In the MTG reactor, the ZSM-5 zeolite catalyst is employed, and the operation is conducted at almost 21 bar. The inlet and outlet temperatures are 330 and 400 °C, respectively. After product separation, a large gas flow of light hydrocarbons is recycled to the gasoline synthesis reactors to control the temperature rise over the reactors. However, here, to simplify the simulation of the MTG unit in PRs 1 and 2, the plant layout concept has been adapted from the NREL technical report, according to which MeOH is directly fed into a MTG fluidized bed reactor with no cycle gas in the loop.[14,42] A similar product distribution and composition was assumed for the product of the DTG reactor in PR 5 because MTD conversion normally occurs inside the MTG reactor followed by further dehydration reactions toward hydrocarbons.

For PRs 3 and 4, the product distribution in the DTG reactors was adapted from the TIGAS process. In the gasoline synthesis reactor, the conversion of oxygenates to hydrocarbons and water occurs over the GSK-10 zeolite catalyst. The operation is adiabatic and the inlet and outlet temperatures are 349 and 396 °C, respectively.[17] The pressure in the reactor is almost 20 bar,[72] and for this work, the identical pressure as in the MTG reactor was employed. According to the reported block flow diagram of the TIGAS pilot plant, the product mixture leaving the plant contains about 18 wt % water and 82 wt % hydrocarbons including almost 24 wt % gasoline and 76 wt % unconverted and light gases.[17] Since no information on gasoline composition was provided, the same data as used for the MTG reactor were considered, although the quality of synthesized gasoline in DTG plants might be slightly different, especially regarding aromatic content.

From the simulation result of the DTG unit based on the TIGAS process and also knowing that in the MTG plants, the mass yield of produced gasoline is typically around 35% of the MeOH feed, a relationship for gasoline to DME/MeOH was figured out, as indicated by eq 19. The derived equation can estimate the production rate in gasoline synthesis plants via direct STD conversion and can easily be adjusted when new data are available.

$$\dot{m}_{gasoline} = 57.5\%\ \dot{m}_{DME} + 35\%\ \dot{m}_{MeOH} \quad (19)$$

As mentioned before, the validity of the assumptions made for the MTG/DTG reactors was examined by performing atom balances over the reactors and also the whole plant boundary (related to Figure 2). Table 7 represents the atom balance difference over the plant boundary in the selected process routes, and as evident, the results appear satisfactory. It can be seen that the atom balance difference for PRs 1 (or 5) and 2 is below 1%, and for PRs 3 and 4, it shows small deviations, the reason for which is likely due to the assumptions taken in the DTG reactor unit.

https://doi.org/10.1021/acs.energyfuels.3c04524
Energy Fuels XXXX, XXX, XXX−XXX

Table 7. Atom Balance Difference over the Plant Boundary in the Selected Process Routes

PR no.	carbon (%)	hydrogen (%)	oxygen (%)
1	<−1	<+1	<+1
2	−1	0	<+1
3	<−4	<−1	<+2
4	<−4	<−1	<+2
5	<−1	<+1	<+1

4. RESULTS AND DISCUSSION

4.1. Process Route Evaluation. The process routes 1 or 2 (STG via STM), 3 or 4 (STG via direct STD), and 5 (STG via indirect STD) were simulated using an equal amount of syngas feed to the plant with the composition taken from Table 1 (first row). Since the feed flow directed to the WGS unit (HU2) in PRs 1, 3, and 5 is a split from the total feed to the plant, the feed to the reaction unit (HU4) of these process routes decreases. Therefore, generally, the process routes with makeup H_2 supplied from an external source, PRs 2 and 4, lead to a higher productivity than the similar process routes with the internal WGS unit.

The comparison of the process routes in terms of syngas feed conversion shows that generally direct DME synthesis is more advantageous, as the X_{CO} and X_{H2} are obtained to be 48 and 28% in the STM reactor and 77 and 64% in the STD reactor, respectively. As a measure of productivity, the mass and energetic efficiencies of the process routes are compared in Figure 7. Here, makeup H_2 has been accounted for in the calculations related to PRs 2 and 4. At first view, it is apparent that the efficiencies for PRs 1 and 5 are similar because of the identical assumption used for product distribution in both processes as described before. The difference between these two processes is mainly regarding the amount of exothermic reaction heat of the MTG and DTG reactors, such that from the MTG reactor in PR 1, a higher reaction heat is developed compared to the DTG reactor in PR 5 because in the latter, the heat is partially removed beforehand through the MeOH dehydration process in the MTD reactor.

Besides, it can be seen that the results of PRs 3 and 4 are close because due to the lower required amount of makeup H_2 for DME synthesis, the productivity is not that much affected by the source of makeup H_2. The mass efficiencies of the products, DME and gasoline, in PR 3 are 27 and 15%, respectively. In PR 4, the efficiencies are 29 and 16%, respectively. Comparing STG processes via STM and STD syntheses shows that between PRs 1 and 3 with the internal WGS unit for makeup H_2, the STD route is more productive. As mentioned earlier, PR 3 yields a gasoline mass efficiency of 15%, whereas this is about 11% in PR 1. However, between PRs 2 and 4 with added makeup H_2, PR 2 attains a gasoline mass efficiency of approximately 19%, compared to 16% in PR 4. Consequently, the gasoline energetic efficiency in relation to carbon also increases in PR 2, as depicted in Figure 7b. The reason for the better results observed in PR 2 is that in the simulation, the feed amount to the STM reactor in PR 2 including the recycle gas is almost twice the feed amount to the STD reactor in PR 4. If one pass conversion is considered, PR 4 is more productive, but enhancing the overall syngas conversion by cycling back the unconverted gases leads to a significant increase of MeOH production in the STM reactor and consequently a higher product efficiency in PR 2. In summary, it can be concluded that by introducing equal amounts of feed to the reaction units, biofuel synthesis via direct DME synthesis compared to the MeOH synthesis pathway is more productive.

As evident from Figure 7b, when comparing PR 2 and PR 4 based on the syngas enhanced with H_2, PR 4 shows a higher energetic efficiency. The gasoline energetic efficiency in relation to syngas is approximately 65 and 67% in PR 3 and PR 4, respectively, surpassing the results in PR 1 and PR 2, which stand at 50 and 54%, respectively. Considering the superior results obtained in the DTG pathway compared to the MTG pathway, it can be inferred that the product mass and energetic efficiencies with respect to biomass are also higher for the DTG pathway, consistent with the findings reported by Dimitriou et al.[22]

In addition to the productivity, the processes should be eventually evaluated from an economic point of view. One important factor in the economy of biofuel synthesis plants is concerning the H_2 consumption, as the H_2 source and related production method costs are very determinant in the total costs. Since biomass-derived syngas is normally low in H_2, adding makeup H_2 to syngas is inevitable; this is obviously more significant for MeOH synthesis than DME synthesis. The

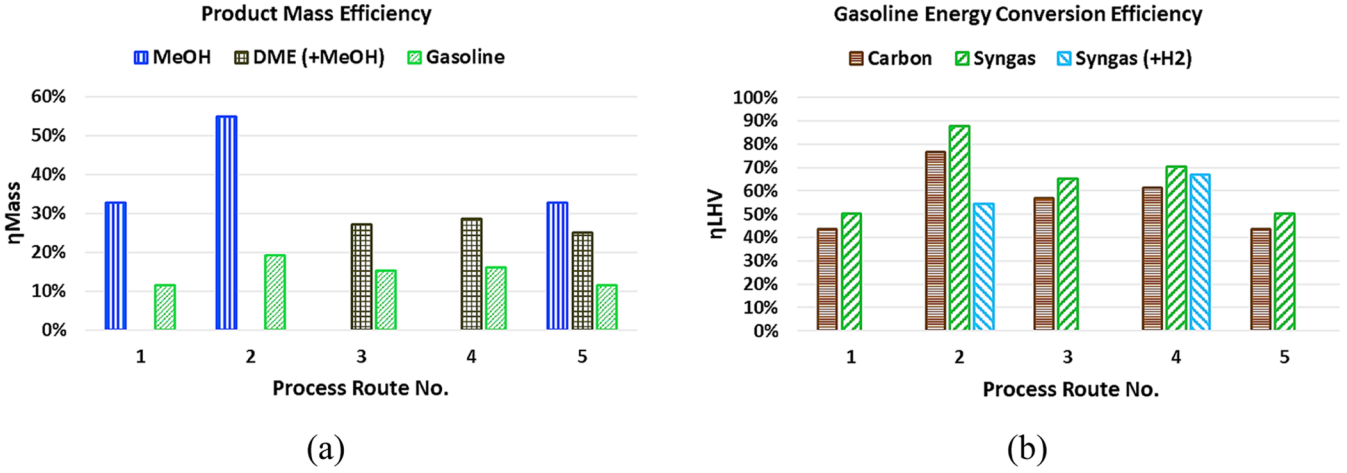

Figure 7. Comparison of (a) mass efficiency of MeOH/DME and gasoline with respect to syngas and (b) energy conversion efficiency of gasoline with respect to syngas and carbon for the selected process routes.

https://doi.org/10.1021/acs.energyfuels.3c04524
Energy Fuels XXXX, XXX, XXX−XXX

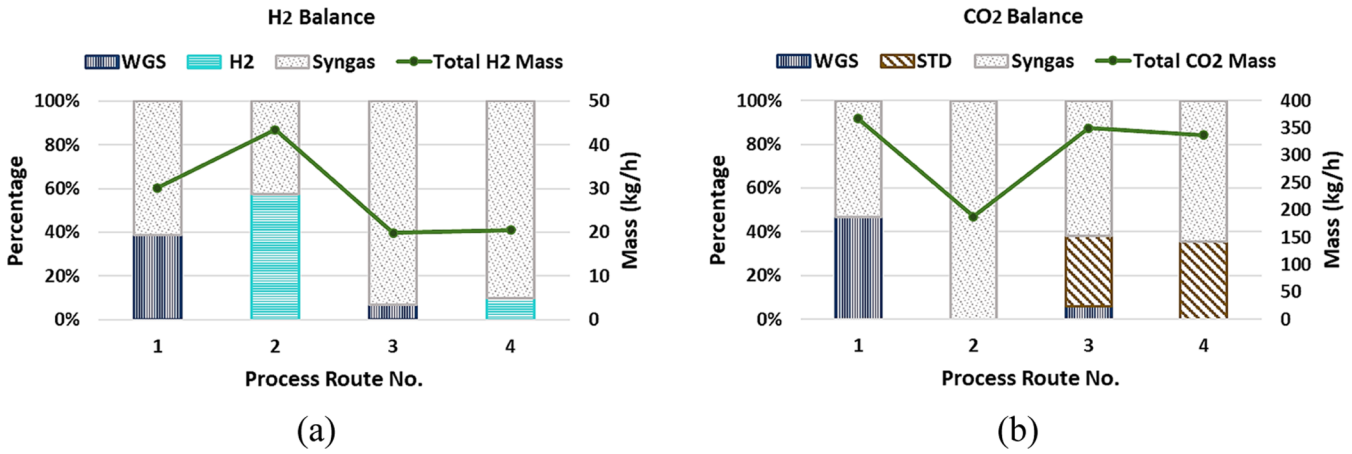

Figure 8. Comparison of (a) H_2 balance and (b) CO_2 balance for the selected process routes.

total amount of consumed H_2, including syngas content and makeup H_2, and also the percentage of the H_2 supply source contributed in each process route are illustrated in Figure 8a, and the H_2 amount per kg product can be seen in Table 8.

Table 8. H_2 Demand of Intermediate and Final Product Synthesis

PR no.	1	2	3	4	5
kg_{H_2}/kg_{MeOH}	0.16	0.15			0.16
$kg_{H_2}/kg_{DME\ (+MeOH)}$			0.15	0.15	0.21
$kg_{H_2}/kg_{gasoline}$	0.46	0.43	0.26	0.26	0.46

CO_2 balance is an important matter of debate also in biofuel synthesis processes with regard to carbon efficiency and CO_2 footprint. Excess CO_2 from syngas feed and the amounts generated in the WGS and STD units are mainly removed in the CO_2 absorption unit. Figure 8b shows the amount of CO_2 exhausted from each process route and also the contribution percentage of the WGS and STD units in CO_2 formation. In general, in STG via the direct STD synthesis process, PR 3 (or 4), the product of the STD reactor along with unconverted and light gases is fed into the DTG reactor, such that a considerable part of this gas is CO_2 as the byproduct of DME synthesis, and hence should be treated in the CO_2 absorption unit before being recycled to the STD reactor. Then, in such plants, due to a high recycle gas flow rate, the capital investment and operating costs are high.[32] On the other hand, in PR 1 (or 2) with STM synthesis, only crude MeOH with the purity of 96 wt % is introduced to the MTG reactor, with no light gases, and contrary to PR 3 (or 4), through the product separation, only a small flow rate of gas (mostly LPG) as the side product of gasoline synthesis leaves the separation unit.

Table 9 specifies the amount of generated CO_2 per kilogram of synthesized gasoline in the process routes. It is considerable that although CO_2 formation via the MeOH synthesis process is lower, generated CO_2 in PR 1 is greater than that in PR 3 (or 4) because of the WGS unit there that should provide the makeup H_2 for MeOH synthesis. Therefore, concerning the CO_2 footprint, it can be inferred that the MTG plants can be more advantageous if H_2 is provided by processes with less or no CO_2 emission.

Table 9. CO_2 Formation Per Kg Product

PR no.	1	2	3	4	5
$kg_{CO_2}/kg_{gasoline}$	6.5	1.9	4.6	4.1	6.5

Sankey diagrams related to Figure 8a,b are available in the Supporting Information.

If the transportability of the intermediate products is the matter, MeOH is a liquid, but DME needs pressurization and liquefaction for transportation. Also, the separation of DME from syngas is much more complicated than MeOH separation. In the case of gasoline synthesis via the MeOH pathway, it is said that the optimum is the production of MeOH in regions with low price energy, ideally from renewable energy sources, and then its transportation to target countries for MTG conversion. Then, for gasoline synthesis via the DME pathway (the bioliq process), it might be more advantageous to consider the plant location more desirably near biomass feedstock fields and eventually the transportation of the finished product of gasoline to the market.

4.2. Scale Up of the Optimized Bioliq Plant. In the previous section, the advantages and disadvantages of the selected process routes were deliberated, and the productivity of the bioliq process toward gasoline production was demonstrated. Subsequently, the process was scaled up for future techno-economic analysis on a larger scale and also for comparison with other processes. Then, the data of PR 3, representing the optimized bioliq process, were used for scaling up. A simulation was performed for an industrial scale-optimized bioliq process for the production of around 100,000 tons of gasoline annually, and accordingly, the process was scaled up for a gasoline production rate of 15−16 t/h (8000 work h/y). The required amount of syngas feed was estimated based on the simulation result of PR 3 and eq 19, and the (optimized) syngas composition was taken from Table 1 (second row). The results of mass and chemical energy balances as well as atom (element) and CO_2 balances are represented by Sankey diagrams given in Figures 9−14. The syngas in the diagrams considers only CO, H_2, and CO_2 components in the streams.

According to Figure 9, the mass yields of the intermediate product of DME (plus MeOH) and gasoline with respect to syngas are approximately 28 and 16%, respectively, similar to the results obtained in PR 3 (Figure 7a). The energy conversion efficiencies, illustrated in Figure 10, for synthesized DME (plus MeOH) and gasoline are about 77 and 66%,

https://doi.org/10.1021/acs.energyfuels.3c04524
Energy Fuels XXXX, XXX, XXX−XXX

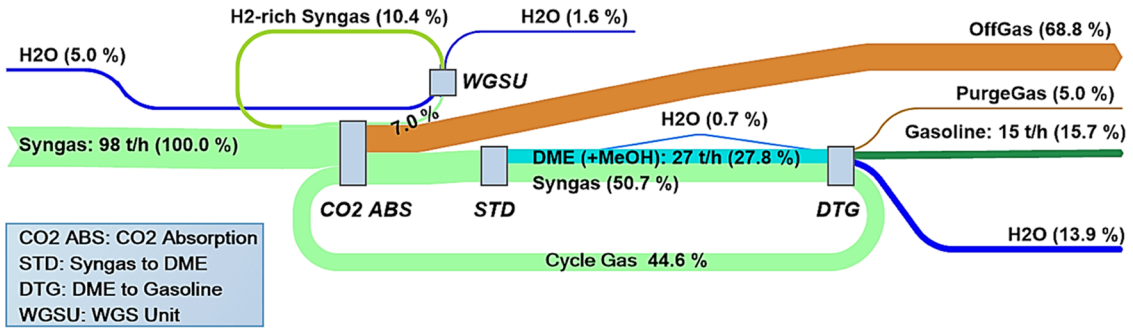

Figure 9. Scaled-up bioliq plant, mass balance diagram.

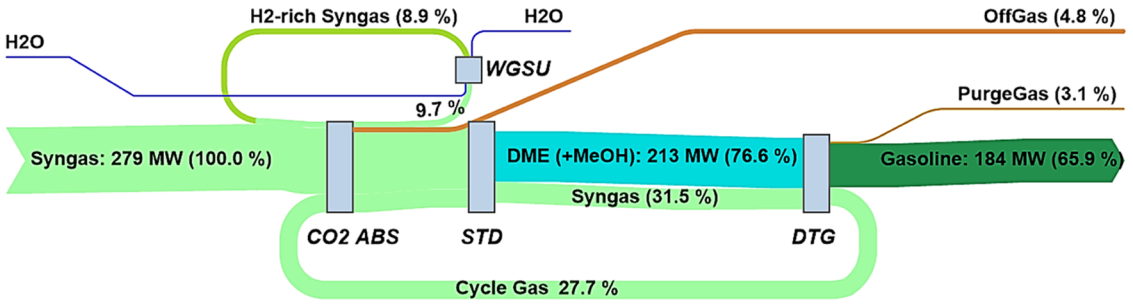

Figure 10. Scaled-up bioliq plant, chemical energy balance diagram.

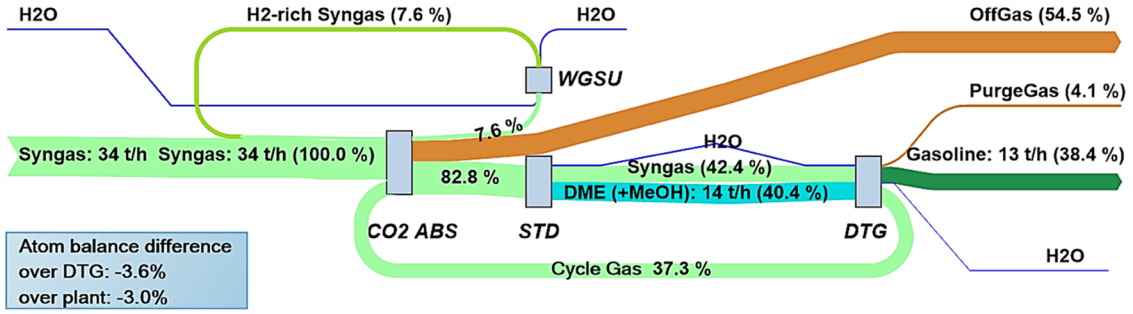

Figure 11. Scaled-up bioliq plant, carbon balance diagram.

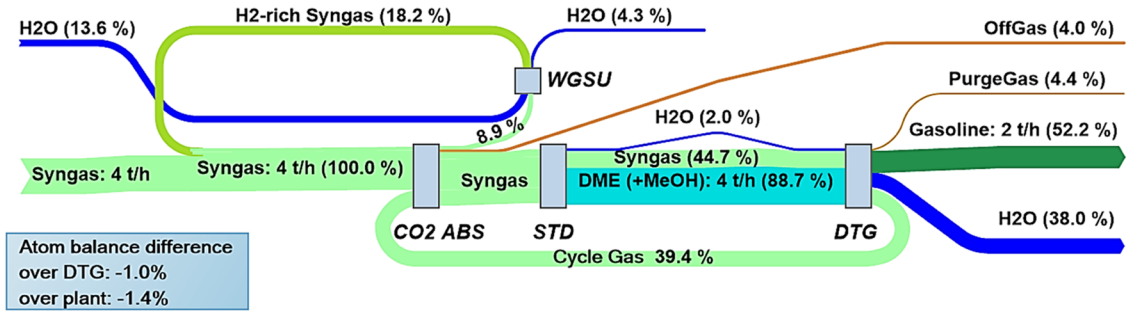

Figure 12. Scaled-up bioliq plant, hydrogen balance diagram.

respectively. These efficiencies are higher compared to those in the MTG pathway, as discussed earlier. The atom balance diagrams for carbon, hydrogen, and oxygen elements are visualized by Figures 11−13, respectively. As can be seen in all diagrams, the atom balance difference remains below 4% for the DTG reactor unit and below 3% for the entire plant boundary. Overall, it can be deduced that the assumptions made for the DTG reactor is quantitatively reasonable, although the composition of gasoline from an actual DTG plant might not be exactly alike to MTG plants. From the carbon balance diagram (Figure 11), it is clear that the overall carbon conversion efficiency is about 38%, and as expected, the carbon lost from off-gas is considerable due to the large CO_2 release. As can be seen in Figure 14, less than 50% of the CO_2 leaving the plant is generated within the plant, while over 50% originates from the CO_2 content of syngas, which is subject to the nature of feedstock and the gasification process. As evident in Figure 12, the H_2 efficiency stands at approximately 52%, while 38% of the feed H_2 content is observed as the side

https://doi.org/10.1021/acs.energyfuels.3c04524
Energy Fuels XXXX, XXX, XXX−XXX

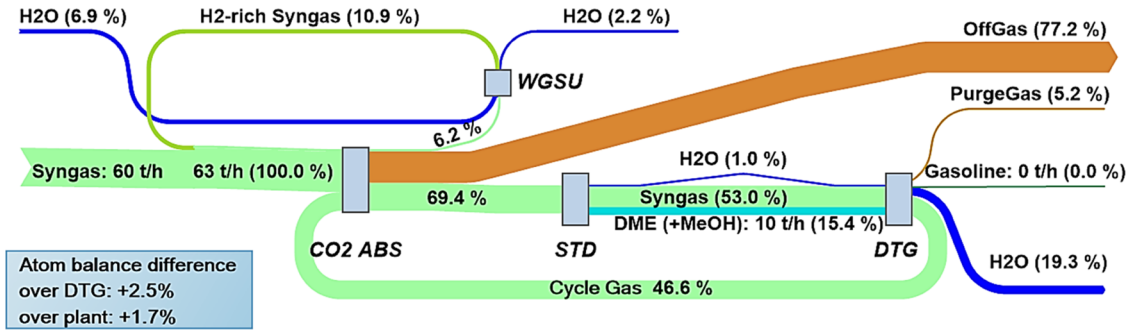

Figure 13. Scaled-up bioliq plant, oxygen balance diagram.

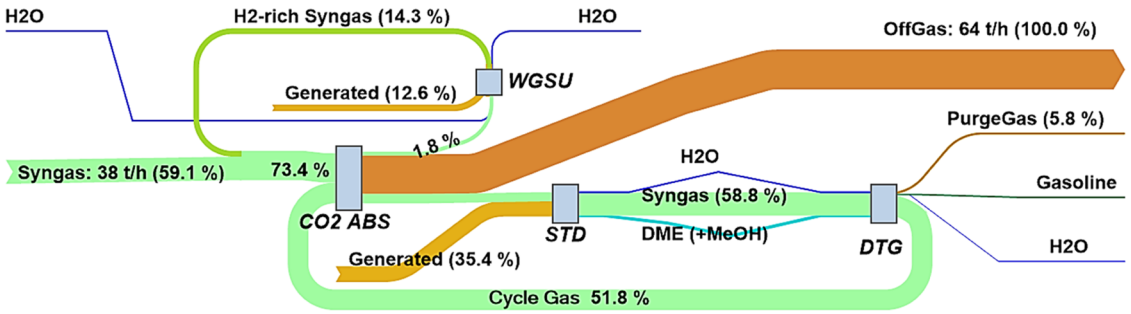

Figure 14. Scaled-up bioliq plant, CO_2 balance diagram.

product water. Figure 13 illustrates the O_2 balance as a part of the atom balance calculations.

The mass and chemical energy efficiencies (eqs 17 and 18) for the gasoline product with respect to biomass (dry) were calculated to be about 13 and 35%, respectively. For a comparable process but through the MTG pathway, these efficiencies are estimated to be around 10 and 26%, respectively. These hypothesis data for the MTG pathway were derived from the relationship between intermediate and gasoline product data obtained in PRs 1 and 3. As Dahmen et al.[73] reported, the energetic efficiencies for BTL processes based on straw gasification range from 33 to 39% when the straw water content is between 7% and 10 wt %. Also, based on the reported data, the mass yield is from 9 to 12%. Liu et al.[74] simulated the process of converting lignocellulosic biomass (15 wt % moisture) to gasoline through the MTG process, and from their results, mass and energy efficiencies of 15 and 42%, respectively, can be derived. Then, the results of this work align with those of previous studies. Furthermore, it is worth mentioning that the BTL process via straw gasification usually represents lower mass and energetic efficiencies compared to the BTL process via wood gasification due to the lower energy nature of straw. Baliban et al.[75] conducted mass and energy balances for the conversion of hardwood (45 wt % moisture) into liquid transportation fuels through various process routes, and as can be inferred from their results, the mass and energy efficiencies for the liquid fuels (gasoline, diesel, and kerosene) with respect to biomass are around 23−25 and 55−61%, respectively.

The technology readiness level (TRL) for MeOH, DME, and also MTG synthesis is dependent on the synthesis technology and feedstock used in the process. In the case of synthesis from conventional syngas based on natural gas and coal conversion, the production is on a commercial scale and meets the technical maturity of TRL 9; however, the synthesis from biomass-based syngas has lower TRL maturities. The bioliq plant is in operation in pilot scale of around 50 kg/h and has reached the technical maturity of TRL 6.[5]

5. CONCLUSIONS

In this work, five selected process routes for gasoline synthesis from biomass-derived syngas via MeOH and DME pathways have been investigated by process simulation using identical assumptions and conditions in order to guarantee the comparability. The general plant layout was adapted from the bioliq plant and then modified based on the objective of each process route. The STM, MTD, STD, and WGS reactions were simulated using selected LHHW kinetic models. The simulated models were validated using industrial plant data from literature, and it was found that the model of Bussche et al. for MeOH synthesis, Bercic et al. for DME synthesis from MeOH, and a model reported by Lu et al. for WGS synthesis can accurately predict the outcomes of the corresponding reactions. Also, a combined model of Bussche and Bercic showed reasonable results for modeling the direct conversion of syngas to DME.

The simulation results of the selected process routes showed that gasoline synthesis via the direct DME pathway, essentially the original bioliq process, is more productive than the process configuration via the MeOH pathway. Syngas conversion in the STG process via direct DME synthesis is higher compared to the MeOH synthesis route, whereas the GHSV and residence times are kept equivalent in the STM and STD reactors. Moreover, the lower H_2 consumption in DME synthesis makes it a favorable process. Besides, the mass yield of synthesized gasoline to the intermediate product in the STG process via direct DME synthesis is larger than that via MeOH synthesis (see Figure 7a). In MTG reactors, the mass yield of gasoline to MeOH is usually about 35%, and accordingly in the DTG plants with direct DME synthesis, the relationship can be approximated by the derived equation of $\dot{m}_{\text{gasoline}}$ = 57.5%

https://doi.org/10.1021/acs.energyfuels.3c04524
Energy Fuels XXXX, XXX, XXX−XXX

$\dot{m}_{DME}$ + 35% $\dot{m}_{MeOH}$, which was used for scaling up the optimized bioliq process to produce 100,000 t/y of gasoline.

Overall, the bioliq process has a promising future in sustainable biofuels, and the high productivity and low H_2 consumption make it a good competitor to processes with the MeOH synthesis pathway. The process has the potential to be further developed, particularly regarding the issue of generating large amounts of CO_2; for instance, the process can be extended by considering a CO_2 capture and conversion unit in a downstream power-to-liquid process. In conclusion, the selection of the most suitable process constellation relies on the optimization target, whether it is hydrogen consumption, carbon conversion, mass, or energy efficiency. To conduct a more comprehensive analysis of the studied process routes, a techno-economic evaluation will be carried out for the selected routes and also for the scaled-up optimized bioliq process in the next phase of the investigation.

■ ASSOCIATED CONTENT

Supporting Information

The Supporting Information is available free of charge at https://pubs.acs.org/doi/10.1021/acs.energyfuels.3c04524.

Overall flowsheets of simulated PR 1−PR 5 with stream compositions; flowsheets of HU1−HU5 of PR 3 and HU4 of PR 5 with stream compositions; the hydrogen and carbon dioxide balances related to Figure 8; and the reaction kinetic model data with a brief description for specifying LHHW reactions in Aspen Plus (PDF)

■ AUTHOR INFORMATION

Corresponding Authors

Mahsa E-Moghaddam − *Institute of Catalysis Research and Technology (IKFT), Karlsruhe Institute of Technology (KIT), 76344 Karlsruhe, Germany*; orcid.org/0009-0009-6704-6568; Email: mahsa.moghaddam@kit.edu

Nicolaus Dahmen − *Institute of Catalysis Research and Technology (IKFT), Karlsruhe Institute of Technology (KIT), 76344 Karlsruhe, Germany*; Email: nicolaus.dahmen@kit.edu

Authors

Ulrike Santo − *Institute for Technical Chemistry (ITC), Karlsruhe Institute of Technology (KIT), 76021 Karlsruhe, Germany*

Jörg Sauer − *Institute of Catalysis Research and Technology (IKFT), Karlsruhe Institute of Technology (KIT), 76344 Karlsruhe, Germany*; orcid.org/0000-0003-3133-4110

Complete contact information is available at: https://pubs.acs.org/10.1021/acs.energyfuels.3c04524

Notes

The authors declare no competing financial interest.

■ ACKNOWLEDGMENTS

This work was created, thanks to the support of the Strategy Dialogue Automotive Industry SDA and the Ministry of Transport of Baden Württemberg as part of the project "Rethinking reFuels fuels".

■ NOMENCLATURE

Abbreviations and Subscripts

BTL fuels, biomass-to-liquid fuels; DTG, dimethyl ether to gasoline; HT, high temperature; HU, hierarchy unit; LHV, lower heating value; LT, low temperature; MTD, methanol to dimethyl ether; MTG, methanol to gasoline; PR, process route; SN, stoichiometric number; STD, syngas to dimethyl ether; STM, syngas to methanol; STG, syngas to gasoline; WGS, water−gas shift; in, inlet; out, outlet; Rea, reactant; Pro, product; ref, reference

Symbols and Greek Letters

$\dot{m}$, mass flow rate; $\dot{n}$, mole flow rate; $\dot{V}_{feed,st}$, volumetric flow rate of feed in standard condition; V_{cat}, volume of catalyst

■ REFERENCES

(1) Mat Aron, N. S.; Khoo, K. S.; Chew, K. W.; Show, P. L.; Chen, W.-H.; Nguyen, T. H. P. Sustainability of the four generations of biofuels − A review. *Int. J. Energy Res.* **2020**, *44* (12), 9266−9282.

(2) Verger, T.; Azimov, U.; Adeniyi, O. Biomass-based fuel blends as an alternative for the future heavy-duty transport: A review. *Renewable Sustainable Energy Rev.* **2022**, *161*, No. 112391.

(3) Dahmen, N.; Dinjus, E.; Kolb, T.; Arnold, U.; Leibold, H.; Stahl, R. State of the art of the bioliq® process for synthetic biofuels production. *Environ. Prog. Sustainable Energy* **2012**, *31* (2), 176−181.

(4) Kolb, T.; Eberhard, M.; Dahmen, N., Ed. *BtL - The bioliq Process at KIT:New Technologies and Alternative Feedstocks in Petrochemistry and Refining*; Vol. 9; DGMK Tagungsbericht, 2013.

(5) Dahmen, N.; Abeln, J.; Eberhard, M.; Kolb, T.; Leibold, H.; Sauer, J.; Stapf, D.; Zimmerlin, B. The bioliq process for producing synthetic transportation fuels. *WIREs Energy Environ.* **2017**, *6* (3), No. e236, DOI: 10.1002/wene.236.

(6) Dahmen, N.; Henrich, E.; Henrich, T. Synthesis gas biorefinery. *Biochem. Eng./Biotechnol.* **2019**, *166*, 217−245.

(7) Weih, N.; Niebel, A.; Pfitzer, C.; Funke, A.; Parku, G. K.; Dahmen, N. Operational experience with miscanthus feedstock at the bioliq fast pyrolysis plant. *J. Anal. Appl. Pyrolysis* **2024**, *177*, No. 106338.

(8) Pfitzer, C.; Dahmen, N.; Tröger, N.; Weirich, F.; Sauer, J.; Günther, A.; Müller-Hagedorn, M. Fast Pyrolysis of Wheat Straw in the Bioliq Pilot Plant. *Energy Fuels* **2016**, *30* (10), 8047−8054.

(9) Niebel, A.; Funke, A.; Pfitzer, C.; Dahmen, N.; Weih, N.; Richter, D.; Zimmerlin, B. Fast Pyrolysis of Wheat Straw—Improvements of Operational Stability in 10 Years of Bioliq Pilot Plant Operation. *Energy Fuels* **2021**, *35* (14), 11333−11345.

(10) Mesfun, S. A. *BIOMASS TO LIQUIDS (BTL) VIA FISCHER - TROPSCH A BRIEF REVIEW:Prepared with the support of project ETIP-B-SABS2*, 2021. https://www.etipbioenergy.eu/images/ETIP_B_Factsheet_BtL_2021.pdf.

(11) Okoye-Chine, C. G.; Gorimbo, J.; Moyo, M.; Yao, Y.; Liu, X.; Hildebrandt, D.; Fox, J. A. *Chemical and Fuels from Biomass via Fischer-Tropsch synthesis:A Route to Sustainability; Catalysis Series No. 44*; Royal Society of Chemistry, 2023.

(12) Morandin, M.; Harvey, S.Methanol via biomass gasification. Thermodynamic performances and process integration aspects in Swedish chemical cluster and pulp and paper sites, 2015. DOI: 10.13140/RG.2.1.4272.1443.

(13) Bozzano, G.; Manenti, F. Efficient methanol synthesis: Perspectives, technologies and optimization strategies. *Prog. Energy Combust. Sci.* **2016**, *56*, 71−105.

(14) Schreiner, M. *Research guidance studies to assess gasoline from coal by methanol-to-gasoline and sasol-type Fischer-Tropsch technologies*, 1978. https://www.osti.gov/servlets/purl/6348367.

(15) Stiefel, M.; Ahmad, R.; Arnold, U.; Döring, M. Direct synthesis of dimethyl ether from carbon-monoxide-rich synthesis gas: Influence of dehydration catalysts and operating conditions. *Fuel Process. Technol.* **2011**, *92* (8), 1466−1474.

(16) Bozga, G.; Apan, I. T.; Bozga, R. E. Dimethyl Ether Synthesis Catalysts, Processes and Reactors. *RPCAT* **2013**, *2* (1), 68−81.
(17) Udengaard, N.; Knight, R.; Wendt, J.; Patel, J.; Walston, K.; Jokela, P.; Adams, C. *Green gasoline from wood using carbona gasification and topsoe TIGAS process.:(No. DOE-TOPSOE-EE0002874-F)*, 2015. https://www.osti.gov/servlets/purl/1173129.
(18) Kim, Y.-D.; Yang, C.-W.; Kim, B.-J.; Moon, J.-H.; Jeong, J.-Y.; Jeong, S.-H.; Lee, S.-H.; Kim, J.-H.; Seo, M.-W.; Lee, S.-B.; Kim, J.-K.; Lee, U.-D. Fischer−tropsch diesel production and evaluation as alternative automotive fuel in pilot-scale integrated biomass-to-liquid process. *Appl. Energy* **2016**, *180*, 301−312.
(19) Baliban, R. C.; Elia, J. A.; Floudas, C. A. Biomass to liquid transportation fuels (BTL) systems: process synthesis and global optimization framework. *Energy Environ. Sci.* **2013**, *6* (1), 267−287.
(20) Trippe, F.; Fröhling, M.; Schultmann, F.; Stahl, R.; Henrich, E.; Dalai, A. Comprehensive techno-economic assessment of dimethyl ether (DME) synthesis and Fischer−Tropsch synthesis as alternative process steps within biomass-to-liquid production. *Fuel Process. Technol.* **2013**, *106*, 577−586.
(21) Iglesias Gonzalez, M.; Kraushaar-Czarnetzki, B.; Schaub, G. Process comparison of biomass-to-liquid (BtL) routes Fischer−Tropsch synthesis and methanol to gasoline. *Biomass Convers. Biorefin.* **2011**, *1* (4), 229−243.
(22) Dimitriou, I.; Goldingay, H.; Bridgwater, A. V. Techno-economic and uncertainty analysis of Biomass to Liquid (BTL) systems for transport fuel production. *Renewable Sustainable Energy Rev.* **2018**, *88*, 160−175.
(23) Wang, Z.; He, T.; Li, J.; Wu, J.; Qin, J.; Liu, G.; Han, D.; Zi, Z.; Li, Z.; Wu, J. Design and operation of a pilot plant for biomass to liquid fuels by integrating gasification, DME synthesis and DME to gasoline. *Fuel* **2016**, *186*, 587−596.
(24) Ibarra-Gonzalez, P.; Rong, B.-G. Integrated Methodology for Optimal Synthesis of Lignocellulosic Biomass-to-Liquid Fuel Production Processes: 2. Superstructure MINLP Modeling and Evaluation for Optimal Biofuel Process Synthesis and Integration. *Ind. Eng. Chem. Res.* **2020**, *59* (33), 14898−14913.
(25) Field, R. P.; Brasington, R. Baseline Flowsheet Model for IGCC with Carbon Capture. *Ind. Eng. Chem. Res.* **2011**, *50* (19), 11306−11312.
(26) Graaf, G. H.; Sijtsema, P. J. J. M.; Stamhuis, E. J.; Joosten, G. E. H. Chemical equilibria in methanol synthesis. *Chem. Eng. Sci.* **1986**, *41*, 2883−2890.
(27) Graaf, G. H.; Stamhuis, E. J.; Beenackers, A. A. C. M. Kinetics of low-pressure methanol synthesis. *Chem. Eng. Sci.* **1988**, *43*, 3185−3195.
(28) Graaf, G. H.; Scholtens, H.; Stamhuis, E. J.; Beenackers, A. A. C. M. Intra-particle diffusion limitations in low-pressure methanol synthesis. *Chem. Eng. Sci.* **1990**, *45*, 773−783.
(29) Bussche, K.; Froment, G. F. A Steady-State Kinetic Model for Methanol Synthesis and the Water Gas Shift Reaction on a Commercial Cu/ZnO/Al2O3Catalyst. *J. Catal.* **1996**, *161* (1), 1−10.
(30) Bercic, G.; Levec, J. Catalytic dehydration of methanol to dimethyl ether. Kinetic investigation and reactor simulation. *Ind. Eng. Chem. Res.* **1993**, *32* (11), 2478−2484.
(31) Diep, B. T.; Wainwright, M. S. Thermodynamic equilibrium constants for the methanol-dimethyl ether-water system. *J. Chem. Eng. Data* **1987**, *32* (3), 330−333.
(32) Lu, W.-Z.; Teng, L.-H.; Xiao, W.-D. Simulation and experiment study of dimethyl ether synthesis from syngas in a fluidized-bed reactor. *Chem. Eng. Sci.* **2004**, *59* (22−23), 5455−5464.
(33) Kiss, A. A.; Pragt, J. J.; Vos, H. J.; Bargeman, G.; Groot, M. T. de. Novel efficient process for methanol synthesis by CO 2 hydrogenation. *Chem. Eng. J.* **2016**, *284*, 260−269.
(34) Park, N.; Park, M.-J.; Ha, K.-S.; Lee, Y.-J.; Jun, K.-W. Modeling and analysis of a methanol synthesis process using a mixed reforming reactor: Perspective on methanol production and CO2 utilization. *Fuel* **2014**, *129*, 163−172.
(35) Bartholomew, C. H.; Farrauto, R. J. *Fundamentals of Industrial Catalytic Processes*, 2nd ed.; John Wiley & Sons, 2011.
(36) Song, D.; Cho, S. Y.; Vu, T. T.; Duong, Y. H. P.; Kim, E. Validation of a Fixed Bed Reactor Model for Dimethyl Ether Synthesis Using Pilot-Scale Plant Data. *Catalysts* **2021**, *11* (12), 1522.
(37) Omata, K.; Watanabe, Y.; Umegaki, T.; Ishiguro, G.; Yamada, M. Low-pressure DME synthesis with Cu-based hybrid catalysts using temperature-gradient reactor. *Fuel* **2002**, *81* (11−12), 1605−1609.
(38) Ereña, J.; Garoña, R.; Arandes, J. M.; Aguayo, A. T.; Bilbao, J. Effect of operating conditions on the synthesis of dimethyl ether over a CuO-ZnO-Al2O3/NaHZSM-5 bifunctional catalyst. *Catal. Today* **2005**, *107−108*, 467−473.
(39) Huang, M.-H.; Lee, H.-M.; Liang, K.-C.; Tzeng, C.-C.; Chen, W.-H. An experimental study on single-step dimethyl ether (DME) synthesis from hydrogen and carbon monoxide under various catalysts. *Int. J. Hydrogen Energy* **2015**, *40* (39), 13583−13593.
(40) Zhu, Y.; Wang, S.; Ge, X.; Liu, Q.; Luo, Z.; Cen, K. Experimental study of improved two step synthesis for DME production. *Fuel Process. Technol.* **2010**, *91* (4), 424−429.
(41) Peláez, R.; Marín, P.; Ordóñez, S. Direct synthesis of dimethyl ether from syngas over mechanical mixtures of CuO/ZnO/Al2O3 and γ-Al2O3: Process optimization and kinetic modelling. *Fuel Process. Technol.* **2017**, *168*, 40−49.
(42) Phillips, S. D.; Tarud, J. K.; Biddy, M. J.; Dutta, A. Gasoline from Wood via Integrated Gasification, Synthesis, and Methanol-to-Gasoline Technologies DOI: 10.2172/1004790.
(43) Dieterich, V.; Buttler, A.; Hanel, A.; Spliethoff, H.; Fendt, S. Power-to-liquid via synthesis of methanol, DME or Fischer−Tropsch-fuels: a review. *Energy Environ. Sci.* **2020**, *13* (10), 3207−3252.
(44) Chang, C. D.; Kuo, J.; Lang, W.; Jacob, S.; Wise, J.; Silvestri, A. Process Studies on the Conversion of Methanol to Gasoline. *Ind. Eng. Chem. Process Des. Dev.* **1978**, *17* (3), 255 DOI: 10.1021/i260067a008.
(45) Shoinkhorova, T.; Cordero-Lanzac, T.; Ramirez, A.; Chung, S.; Dokania, A.; Ruiz-Martinez, J.; Gascon, J. Highly Selective and Stable Production of Aromatics via High-Pressure Methanol Conversion. *ACS Catal.* **2021**, *11* (6), 3602−3613.
(46) Golubev, K. B.; Bedenko, S. P.; Budnyak, A. D.; Ilolov, A. M.; Tret'yakov, V. F.; Talyshinskii, R. M.; Maksimov, A. L.; Khadzhiev, S. N. Conversion of Oxygenates to Aromatic Hydrocarbons on a Commercial Zeolite Catalyst: Comparison of Ethanol and Dimethyl Ether. *Russ. J. Appl. Chem.* **2019**, *92* (7), 918−923.
(47) Tremel, A.; Wasserscheid, P.; Baldauf, M.; Hammer, T. Techno-economic analysis for the synthesis of liquid and gaseous fuels based on hydrogen production via electrolysis. *Int. J. Hydrogen Energy* **2015**, *40* (35), 11457−11464.
(48) Slotboom, Y.; Bos, M. J.; Pieper, J.; Vrieswijk, V.; Likozar, B.; Kersten, S.; Brilman, D. Critical assessment of steady-state kinetic models for the synthesis of methanol over an industrial Cu/ZnO/Al2O3 catalyst. *Chem. Eng. J.* **2020**, *389*, No. 124181.
(49) Ott, J.; Gronemann, V.; Pontzen, F.; Fiedler, E.; Grossmann, G.; Kersebohm, D. B.; Witte, C., Ed. *Methanol*; Ullmann's Encyclopedia of Industrial Chemistry, 2000.
(50) Graaf, G. H.; Winkelman, J. G. M. Chemical Equilibria in Methanol Synthesis Including the Water−Gas Shift Reaction: A Critical Reassessment. *Ind. Eng. Chem. Res.* **2016**, *55* (20), 5854−5864.
(51) Bisotti, F.; Fedeli, M.; Prifti, K.; Galeazzi, A.; Dell'Angelo, A.; Barbieri, M.; Pirola, C.; Bozzano, G.; Manenti, F. Century of Technology Trends in Methanol Synthesis: Any Need for Kinetics Refitting? *Ind. Eng. Chem. Res.* **2021**, *60* (44), 16032−16053.
(52) Bisotti, F.; Fedeli, M.; Prifti, K.; Galeazzi, A.; Dell'Angelo, A.; Manenti, F. Impact of Kinetic Models on Methanol Synthesis Reactor Predictions: In Silico Assessment and Comparison with Industrial Data. *Ind. Eng. Chem. Res.* **2022**, *61* (5), 2206−2226.
(53) Lacerda de Oliveira Campos, B.; John, K.; Beeskow, P.; Herrera Delgado, K.; Pitter, S.; Dahmen, N.; Sauer, J. A Detailed Process and Techno-Economic Analysis of Methanol Synthesis from H2 and CO2 with Intermediate Condensation Steps. *Processes* **2022**, *10* (8), 1535.

https://doi.org/10.1021/acs.energyfuels.3c04524
Energy Fuels XXXX, XXX, XXX−XXX

(54) Chen, L.; Jiang, Q. Z.; Song, Z. Z.; Chen, L. Optimization of Inlet Temperature of Methanol Synthesis Reactor of LURGI Type. *AMR* **2012**, *443−444*, 671−677.
(55) Chen, L.; Jiang, Q.; Song, Z.; Posarac, D. Optimization of Methanol Yield from a Lurgi Reactor. *Chem. Eng. Technol.* **2011**, *34* (5), 817−822.
(56) Nestler, F.; Schütze, A. R.; Ouda, M.; Hadrich, M. J.; Schaadt, A.; Bajohr, S.; Kolb, T. Kinetic modelling of methanol synthesis over commercial catalysts: A critical assessment. *Chem. Eng. J.* **2020**, *394*, No. 124881.
(57) Bateni, H.; Able, C. Development of Heterogeneous Catalysts for Dehydration of Methanol to Dimethyl Ether: A Review. *Catal. Ind.* **2019**, *11* (1), 7−33.
(58) Pontzen, F.; Liebner, W.; Gronemann, V.; Rothaemel, M.; Ahlers, B. CO2-based methanol and DME − Efficient technologies for industrial scale production. *Catal. Today* **2011**, *171* (1), 242−250.
(59) Farsi, M.; Eslamloueyan, R.; Jahanmiri, A. Modeling, simulation and control of dimethyl ether synthesis in an industrial fixed-bed reactor. *Chem. Eng. Process.: Process Intensif.* **2011**, *50* (1), 85−94.
(60) Farsi, M.; Jahanmiri, A.; Eslamloueyan, R. Modeling and Optimization of MeOH to DME in Isothermal Fixed-bed Reactor *Int. J. Chem. React. Eng.* 2010; Vol. *8* 1 DOI: 10.2202/1542-6580.2063.
(61) Guffanti, S.; Visconti, C. G.; Groppi, G. Model Analysis of the Effects of Active Phase Distribution at the Pellet Scale in Catalytic Reactors for the Direct Dimethyl Ether Synthesis. *Ind. Eng. Chem. Res.* **2020**, *59* (32), 14252−14266.
(62) Rostrup-Nielsen, T.; Nielsen, P.; Joensen, F.; Madsen, J., Eds.; *Polygeneration − Integration of Gasoline Synthesis and IGCC Power Production Using Topsoe's TIGAS Process*, 2007.
(63) Mevawala, C.; Jiang, Y.; Bhattacharyya, D. Techno-economic optimization of shale gas to dimethyl ether production processes via direct and indirect synthesis routes. *Appl. Energy* **2019**, *238*, 119−134.
(64) Boymans, E. H.; Liakakou, E. T. *Advanced liquid biofuels synthesis:Adding value to biomass gasification*, 2018. https://publications.tno.nl/publication/34629460/dQ3r61/e17057.pdf (accessed Oct 30, 2023).
(65) Chen, W.-H.; Hsu, C.-L.; Wang, X.-D. Thermodynamic approach and comparison of two-step and single step DME (dimethyl ether) syntheses with carbon dioxide utilization. *Energy* **2016**, *109*, 326−340.
(66) Sun, J.; Yang, G.; Yoneyama, Y.; Tsubaki, N. Catalysis Chemistry of Dimethyl Ether Synthesis. *ACS Catal.* **2014**, *4* (10), 3346−3356.
(67) Deutschmann, O.; Knözinger, H.; Kochloefl, K.; Turek, T., Eds.; *Heterogeneous Catalysis and Solid Catalysts, 3. Industrial Applications*; Ullmann's Encyclopedia of Industrial Chemistry, 2000.
(68) Barbieri, G. Water Gas Shift (WGS). *Encyclopedia of Membranes* **2016**, 1990−1992.
(69) Alhabdan, F. M. Computer Simulation of Industrial Low Temperature Shift Reactor for the Purification of Syngas. *J. King Saud Univ., Eng. Sci.* **1990**, *2* (1), 73−97.
(70) Choi, Y.; Stenger, H. G. Water gas shift reaction kinetics and reactor modeling for fuel cell grade hydrogen. *J. Power Sources* **2003**, *124* (2), 432−439.
(71) Mendes, D.; Mendes, A.; Madeira, L. M.; Iulianelli, A.; Sousa, J. M.; Basile, A. The water-gas shift reaction: from conventional catalytic systems to Pd-based membrane reactors-a review. *Asia-Pac. J. Chem. Eng.* **2010**, *5* (1), 111−137.
(72) Litvinenko, V.; Meyer, B. *Syngas Production: Status and Potential for Implementation in Russian Industry*; Springer International Publishing, 2018.
(73) Dahmen, N.; Sauer, J. Evaluation of Techno-Economic Studies on the bioliq Process for Synthetic Fuels Production from Biomass. *Processes* **2021**, *9* (4), 684.
(74) Liu, G.; Larson, E. D.; Williams, R. H.; Guo, X. Gasoline from Coal and/or Biomass with CO 2 Capture and Storage. 1. Process Designs and Performance Analysis. *Energy Fuels* **2015**, *29* (3), 1830−1844.
(75) Baliban, R. C.; Elia, J. A.; Floudas, C. A.; Gurau, B.; Weingarten, M. B.; Klotz, S. D. Hardwood Biomass to Gasoline, Diesel, and Jet Fuel: 1. Process Synthesis and Global Optimization of a Thermochemical Refinery. *Energy Fuels* **2013**, *27* (8), 4302−4324.

https://doi.org/10.1021/acs.energyfuels.3c04524
Energy Fuels XXXX, XXX, XXX−XXX